Magnetic excitations in rare-earth-based high-temperature superconductors

1998 J. Phys.: Condens. Matter 10 2579

(http://iopscience.iop.org/0953-8984/10/12/003)

J. Phys.: Condens. Matter **10** (1998) 2579–2596. Printed in the UK PII: S0953-8984(98)82572-1

REVIEW ARTICLE

Magnetic excitations in rare-earth-based high-temperature superconductors

Wolfgang Henggeler and Albert Furrer

Laboratory for Neutron Scattering, Eidgenössische Technische Hochschule Zürich and Paul Scherrer Institut, CH-5232 Villigen PSI, Switzerland

Received 8 December 1997

Abstract. The unique character of inelastic neutron scattering in the study of magnetic excitations of rare-earth-containing high-temperature superconductors is summarized. It is exemplified for single-ion, cluster and collective magnetic excitations which are directly related to the fundamental interactions associated with the rare-earth sublattice. Crystalline-electric-field and cluster excitations are discussed for $Ho_xY_{1-x}Ba_2Cu_3O_7$ which provide information on the electrostatic potential and the magnetic pair coupling at the rare-earth site, respectively. The study of collective magnetic excitations in both grain-aligned samples ($HoBa_2Cu_3O_7$) and single crystals ($Nd_{2-x}Ce_xCuO_4$) yields more detailed information on the exchange coupling. In particular, we show how Ce doping affects the spin-wave dispersion of Nd_2CuO_4, i.e., a strong softening of the excitation spectra is observed which explains the huge Sommerfeld coefficients in $Nd_{2-x}Ce_xCuO_4$ ($x > 0.1$).

Contents

1. Introduction

A large number of high-temperature superconducting materials contain rare-earth (R) ions. The most prominent examples are the hole-doped $RBa_2Cu_3O_7$ and the electron-doped $R_{2-x}Ce_xCuO_4$ compounds. Soon after the first synthesis of the $YBa_2Cu_3O_7$ substance [1, 2] it was realized that Y can be replaced by rare-earth ions, except for R = Tb, Ce. In contrast to conventional superconductors, a coexistence of superconductivity (except for R = Pr) and long-range magnetic order of the R sublattice was observed. In the $R_{2-x}Ce_xCuO_4$ materials crystallizing in the T′ structure superconductivity has been found for R = Pr, Nd, Sm and

0953-8984/98/122579+18$19.50

Eu [3]. In the case of R = Nd and Sm, the R ions show long-range antiferromagnetic order coexisting with superconductivity. In $Nd_{2-x}Ce_xCuO_4$ the rare-earth magnetism leads moreover to a huge linear term in specific heat at low temperatures [4].

To understand the intriguing coexistence of long-range magnetic order and superconductivity in copper-oxide perovskites as well as the heavy-fermion-like behaviour in $Nd_{2-x}Ce_xCuO_4$, detailed knowledge of the magnetic properties of the rare-earth sublattice is required. Essential information on the rare-earth magnetism becomes available through neutron-scattering studies. For most of the known rare-earth-based high-T_c superconductors, the static order of the rare-earth magnetic moments has been established by neutron diffraction. Inelastic neutron scattering (INS) gives direct information on the crystalline-electric-field (CEF) interaction at the R site which defines the magnetic single-ion properties. Moreover, a measurement of the wave-vector dependence of the magnetic excitation energies allows the determination of the exchange-coupling constants between the magnetic moments of the R ions.

In the present work we present different examples of INS experiments on rare-earth-based superconductors which demonstrate the potential of inelastic neutron scattering in the study of these compounds. The cross-section for magnetic neutron scattering is given in section 2 which constitutes the basis for the interpretation of experimental data of single-ion excitations, cluster excitations and collective excitations as exemplified for $Ho_xY_{1-x}Ba_2Cu_3O_7$ and $Nd_{2-x}Ce_xCuO_4$ in sections 3–5, respectively. Some final conclusions are given in section 6.

2. Neutron cross-section for magnetic neutron scattering

Experimental results obtained by inelastic magnetic neutron scattering are most conveniently analysed according to the cross-section formula [5]

$$\frac{\mathrm{d}^2\sigma}{\mathrm{d}\Omega\,\mathrm{d}\omega} = (\gamma r_0)^2 \frac{k'}{k} F^2(\boldsymbol{Q}) \exp\{-2W(\boldsymbol{Q})\} \sum_{\alpha,\beta} \left(\delta_{\alpha\beta} - \frac{Q_\alpha Q_\beta}{Q^2}\right) S^{\alpha\beta}(\boldsymbol{Q},\omega) \tag{1}$$

where $S^{\alpha\beta}(\boldsymbol{Q},\omega)$ is the magnetic scattering function:

$$S^{\alpha\beta}(\boldsymbol{Q},\omega) = \sum_{i,j} \exp\{\mathrm{i}\boldsymbol{Q}\cdot(\boldsymbol{R}_i - \boldsymbol{R}_j)\} \sum_{\lambda,\lambda'} p_\lambda \langle\lambda|\hat{S}_i^\alpha|\lambda'\rangle\langle\lambda'|\hat{S}_j^\beta|\lambda\rangle \delta(\hbar\omega + E_\lambda - E_{\lambda'}). \tag{2}$$

$\gamma = -1.91$ is the gyromagnetic ratio of the neutron, $r_0 = 0.282 \times 10^{-12}$ cm the classical electron radius, k and k' the wavenumbers of the incoming and scattered neutrons, respectively, $\boldsymbol{Q}$ the scattering vector, $F(\boldsymbol{Q})$ the dimensionless magnetic form factor defined as the Fourier transform of the normalized spin density associated with the magnetic ions, $\exp\{-2W(\boldsymbol{Q})\}$ the Debye–Waller factor, $|\lambda\rangle$ and $|\lambda'\rangle$ the initial and final states of the sample with energies E_λ and $E_{\lambda'}$, respectively, p_λ the thermal population factor, and $\hat{S}_i^\alpha$ ($\alpha = x, y, z$) the spin operator of the ith ion at site $\boldsymbol{R}_i$.

There are two factors which govern the cross section (1) in a characteristic way: Firstly, the magnetic form factor $F(\boldsymbol{Q})$ which usually falls off with increasing modulus of the scattering vector $\boldsymbol{Q}$. Secondly, the polarization factor $(\delta_{\alpha\beta} - Q_\alpha Q_\beta/Q^2)$ tells us that neutrons can only couple to spin fluctuations perpendicular to $\boldsymbol{Q}$ which unambiguously allows to distinguish between different polarizations. The essential factor, however, is the magnetic scattering function $S^{\alpha\beta}(\boldsymbol{Q},\omega)$ defined by (2). Using the integral representation of the δ-function $S^{\alpha\beta}(\boldsymbol{Q},\omega)$ transforms into a physically transparent form:

$$S^{\alpha\beta}(\boldsymbol{Q},\omega) = \frac{1}{2\pi\hbar} \sum_{i,j} \int_{-\infty}^{+\infty} \exp\{\mathrm{i}\boldsymbol{Q}\cdot(\boldsymbol{R}_i - \boldsymbol{R}_j)\} \langle \hat{S}_i^\alpha(0)\hat{S}_j^\beta(t)\rangle \exp\{-\mathrm{i}\omega t\}\,\mathrm{d}t. \tag{3}$$

$\langle \hat{S}_i^\alpha(0)\hat{S}_j^\beta(t)\rangle$ is the thermal average of the time-dependent spin operators. It corresponds to the van Hove pair correlation function [6], and gives essentially the probability that, if the magnetic moment of the ith ion at site $\boldsymbol{R}_i$ has some specified (vector) value at time zero, then the moment of the jth ion at site $\boldsymbol{R}_j$ has some other specified value at time t. A neutron scattering experiment measures the Fourier transform of the pair correlation function in space and time, which is clearly just what is needed to describe a magnetic system on an atomic scale.

The van Hove representation of the cross section in terms of pair correlation functions is related to the fluctuation-dissipation theorem [5]:

$$S^{\alpha\beta}(\boldsymbol{Q},\omega) = \frac{N\bar{h}}{\pi}\left\{1 - \exp\left(-\frac{\bar{h}\omega}{k_B T}\right)\right\}^{-1} \operatorname{Im}\chi^{\alpha\beta}(\boldsymbol{Q},\omega) \tag{4}$$

where N is the total number of magnetic ions. Physically speaking, the neutron may be considered as a magnetic probe which effectively establishes a frequency- and wave-vector-dependent magnetic field, $H^\beta(\boldsymbol{Q},\omega)$, in the scattering sample, and detects its response, $M^\alpha(\boldsymbol{Q},\omega)$, to this field by

$$M^\alpha(\boldsymbol{Q},\omega) = \chi^{\alpha\beta}(\boldsymbol{Q},\omega)H^\beta(\boldsymbol{Q},\omega) \tag{5}$$

where $\chi^{\alpha\beta}(\boldsymbol{Q},\omega)$ is the generalized magnetic susceptibility tensor. This is really the outstanding property of the neutron in a magnetic scattering measurement, and no other experimental technique is able to provide such detailed microscopic information about magnetic compounds.

(2) and (3) strictly apply to cases where the orbital angular momentum of the magnetic ions is either zero or quenched by the crystal field. An approximate result can be obtained for ions with unquenched orbital moment such as the rare-earth ions for modest values of Q [7]. One has to replace the spin operator $\hat{S}_i^\alpha$ in (2) and (3) by

$$\hat{S}_i^\alpha = \tfrac{1}{2} g \hat{J}_i^\alpha \tag{6}$$

where

$$g = 1 + \frac{J(J+1) - L(L+1) + S(S+1)}{2J(J+1)} \tag{7}$$

is the Landé splitting factor and J the total angular momentum quantum number resulting from the spin–orbit coupling which combines the spin and orbital angular momentum S and L, respectively.

3. Single-ion excitations in $Ho_xY_{1-x}Ba_2Cu_3O_7$

If the coupling between the magnetic ions is weak, we are left with a single-ion problem, thus the excitation energies will be independent of the scattering vector $\boldsymbol{Q}$. Typical examples are rare-earth-based high-temperature superconductors which usually exhibit very low magnetic ordering temperatures. In this case the dominant mechanism is the crystalline electric field (CEF) interaction.

The CEF potential can be described by the Hamiltonian

$$\mathcal{H}_{CEF} = \sum_{n=1}^{6}\sum_{m=0}^{n} A_n^m(\hat{Y}_n^m + \hat{Y}_n^{-m}) \tag{8}$$

where the A_n^m denote the CEF parameters and the $\hat{Y}_n^m$ are spherical tensor operators [8]. The effect of the CEF on the rare- earth ions is to partially or totally remove the $(2J+1)$-fold

degeneracy of the J multiplets, i.e., there is a splitting into different CEF states Γ_i. From the sequence of the energy levels, properly identified by their irreducible representations Γ_i, the CEF potential can be unambiguously determined. For a detailed description of the CEF interaction in high-T_c superconductors we refer to a recent review article [9].

In evaluating the cross-section for the CEF transition $\Gamma_i \rightarrow \Gamma_j$ we start from the scattering law $S^{\alpha\beta}(\boldsymbol{Q}, \omega)$ defined by (2). Since we are dealing with single-ion excitations, we have $i = j$. For N identical magnetic ions we can even drop the index i. $S^{\alpha\beta}(\boldsymbol{Q}, \omega)$ then reduces to

$$S^{\alpha\beta}(\omega) = N p_{\Gamma_i} \langle \Gamma_i | \hat{J}^{\alpha} | \Gamma_j \rangle \langle \Gamma_j | \hat{J}^{\beta} | \Gamma_i \rangle \delta(\hbar\omega + E_{\Gamma_i} - E_{\Gamma_j}) \tag{9}$$

where p_{Γ_i} is the Boltzmann population factor. From the symmetry relations associated with the matrix elements we find the cross section

$$\frac{\mathrm{d}^2\sigma}{\mathrm{d}\Omega\,\mathrm{d}\omega} = N(\tfrac{1}{2}g\gamma r_0)^2 \frac{k'}{k} F^2(\boldsymbol{Q}) \exp\{-2W(\boldsymbol{Q})\} p_{\Gamma_i} \sum_{\alpha} \left(1 - \frac{Q_\alpha^2}{Q^2}\right) |\langle \Gamma_j | \hat{J}^{\alpha} | \Gamma_i \rangle|^2 \times \delta(\hbar\omega + E_{\Gamma_i} - E_{\Gamma_j}). \tag{10}$$

For experiments on polycrystalline material (10) has to be averaged in $\boldsymbol{Q}$ space:

$$\frac{\mathrm{d}^2\omega}{\mathrm{d}\Omega\,\mathrm{d}\omega} = N(\tfrac{1}{2}g\gamma r_0)^2 \frac{k'}{k} F^2(\boldsymbol{Q}) \exp\{-2W(Q)\} p_{\Gamma_i} |\langle \Gamma_j | \hat{\boldsymbol{J}}_{\perp} | \Gamma_i \rangle|^2 \delta(\hbar\omega + E_{\Gamma_i} - E_{\Gamma_j}) \tag{11}$$

where $\hat{\boldsymbol{J}}_{\perp} = \hat{\boldsymbol{J}} - (\hat{\boldsymbol{J}} \cdot \boldsymbol{Q})\boldsymbol{Q}/Q^2$ is the component of the total angular momentum perpendicular to the scattering vector $\boldsymbol{Q}$, and

$$|\langle \Gamma_j | \hat{\boldsymbol{J}}_{\perp} | \Gamma_i \rangle|^2 = \frac{2}{3} \sum_{\alpha} |\langle \Gamma_j | \hat{\boldsymbol{J}}^{\alpha} | \Gamma_i \rangle|^2. \tag{12}$$

Figure 1 shows energy spectra obtained for polycrystalline $HoBa_2Cu_3O_7$ [10]. The CEF interaction of orthorhombic symmetry D_{2h} splits the $(2J + 1)$-fold degeneracy of the ground-state J multiplet $^5I_8$ into 17 singlet states as indicated on top of figure 1. The ten observed ground-state transitions as well as their intensities were sufficient to determine the nine independent CEF parameters (all terms with odd indices n and m vanish) of the Hamiltonian (8). They were used to calculate the magnetization as well as the Schottky anomaly of the heat capacity which turned out to be in good agreement with the experimental data [11]. Moreover, the CEF parameters correctly predict the turnover of the easy axis of magnetization which changes from the a axis for $T \leqslant 100$ K to the c axis for $T > 100$ K as experimentally verified. This means that the electronic ground state of the Ho^{3+} ions is correctly described by the analysis of the CEF spectra as outlined in [10] and [11].

In high-resolution neutron spectroscopic measurements the widths of CEF transitions are usually found to exhibit line broadening. This is exemplified for the lowest-lying CEF transition of $HoBa_2Cu_3O_7$ in figure 2(a). In metallic systems the major sources of line broadening are relaxation effects of the f electrons with the charge carriers; however, this mechanism has to be excluded here since the charge carriers are bound to Cooper pairs located at twice the gap energy Δ above the Fermi level and therefore not available for relaxation mechanisms. The line broadening must then be attributed to magnetic coupling effects between the Ho^{3+} ions, even for a system like $HoBa_2Cu_3O_7$ with an extremely low magnetic ordering temperature of the Ho sublattice [12]. This can immediately be proven by partially replacing the Ho^{3+} ions with 'non-magnetic' Y^{3+} ions as demonstrated in figures 2(b) and 2(c) which show the lowest-lying CEF transition for the corresponding diluted compounds with Ho contents of 10% [13] and 1%, respectively. The effect of dilution is clearly to reduce the intrinsic linewidth of the CEF excitation, see figure 2(c). The

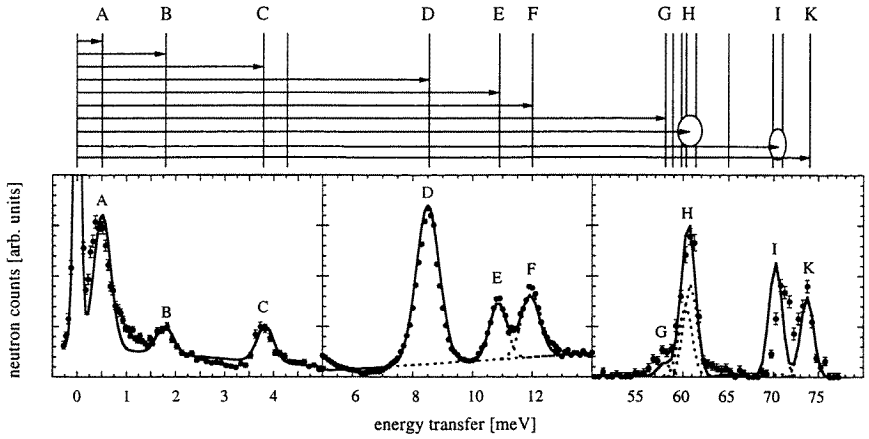

Figure 1. Energy spectra of neutrons scattered from polycrystalline $HoBa_2Cu_3O_7$ at $T = 1.5$ K. The top of the figure shows the resulting sequence of CEF levels.

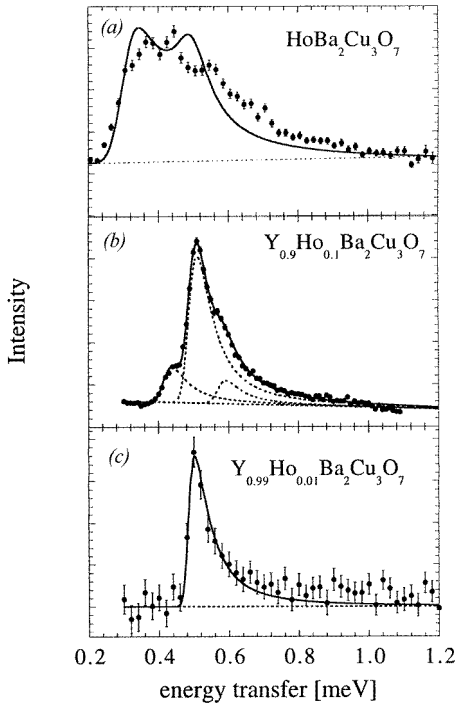

Figure 2. Energy spectra of neutrons scattered from polycrystalline $Ho_xY_{1-x}Ba_2Cu_3O_7$ at $T = 1.5$ K for (*a*) $x = 1$, (*b*) $x = 0.1$ and (*c*) $x = 0.01$.

line drawn in figure 2(a) is a calculation of the expected scattering intensity for the simplified case of isotropic exchange coupling between Ho ions (see section 5.2). A particularly interesting case occurs for 10% Ho content for which the CEF excitation is accompanied by sidelines, see figure 2(b). Assuming a statistical distribution of Ho^{3+} ions we derive

the following cluster probabilities in the (a, b) plane: 66% monomers, 29% dimers and less than 5% trimers, tetramers etc. This means that only two-thirds of the scattering contributes to the central line associated with the single-ion CEF excitations, whereas the sidelines are due to the presence of Ho^{3+} dimers as discussed in the following section.

4. Cluster excitations in $Ho_xY_{1-x}Ba_2Cu_3O_7$

The spin Hamiltonian of a Ho^{3+} dimer in $Ho_xY_{1-x}Ba_2Cu_3O_7$ reads

$$\mathcal{H}_d = \mathcal{H}_{CEF}(1) + \mathcal{H}_{CEF}(2) - 2\mathcal{J}\hat{\boldsymbol{J}}_1 \cdot \hat{\boldsymbol{J}}_2 \tag{13}$$

where the first two terms are given by the single-ion Hamiltonian (8) for a CEF of orthorhombic symmetry D_{2h}, and the third term is the exchange Hamiltonian in the Heisenberg approximation. The symmetry designation of the dimer states is also in D_{2h}. The dimer wavefunctions have the general form

$$|\Gamma_i\rangle = \sum_{J,M} a_i(J_1 J_2 J M)|J_1 J_2 J M\rangle \tag{14}$$

with $\boldsymbol{J} = \boldsymbol{J}_1 + \boldsymbol{J}_2$ and $-J \leqslant M \leqslant J$. Eigenvalues of (13) can be obtained as described in [14]. This is illustrated in figure 3 for both ferromagnetic ($\mathcal{J} > 0$) and antiferromagnetic ($\mathcal{J} < 0$) exchange on the two lowest-lying CEF states Γ_3 and Γ_4. The symmetry properties of the wavefunctions yield the following selection rules for the dimer transitions:

$$|\Gamma_1\rangle \to |\Gamma_2^{(1)}\rangle\colon \Delta J = \pm 1 \qquad \Delta M = \pm 1;\ |\Gamma_1\rangle \to |\Gamma_2^{(2)}\rangle\colon \Delta J = 0 \qquad \Delta M = \pm 1.$$

Thus both transitions have transverse character ($\Delta M = \pm 1$), but they can be distinguished from each other through the Q dependence of the cross section which can be derived from (1) and (2) by setting $i, j = 1, 2$ and $|\lambda\rangle = |\Gamma_i\rangle$. For polycrystalline material we find

$$\frac{\mathrm{d}^2\sigma}{\mathrm{d}\Omega\,\mathrm{d}\omega} = N(\gamma r_0)^2 \frac{k'}{k} F^2(Q) \exp\{-2W(Q)\} p_{\Gamma_i} I_{\Delta J}^{\Delta M}(Q) |\langle \Gamma_j \| \hat{T}^{\Delta M} | \Gamma_i \rangle|^2 \delta(\hbar\omega + E_i - E_j). \tag{15}$$

with

$$I_{\Delta J}^{\Delta M=\pm 1}(Q) = \tfrac{2}{3} - (-1)^{\Delta J}\left[\frac{\sin(QR)}{(QR)^3} - \frac{\cos(QR)}{(QR)^2} - \frac{\sin(QR)}{QR}\right]$$

$$\hat{T}^0 = \hat{J}^z \qquad \hat{T}^{\pm 1} = \mp\tfrac{1}{\sqrt{2}}(\hat{J}^x \pm \hat{J}^y)$$

where N is the total number of dimers and R denotes the separation between the two Ho^{3+} ions within the dimer. The structure factor $I_{\Delta J}^{\Delta M=\pm 1}$ is illustrated in figure 4.

The Q dependence of the two observed dimer transitions does not exhibit the oscillatory nature predicted by the cross-section formula (15), but rather shows the conventional form-factor behaviour [13]. This apparent discrepancy can be explained by the fact that the coupling of the Ho^{3+} ions along the a axis is ferromagnetic, whereas it is antiferromagnetic along the b axis, as evidenced by neutron diffraction studies [12]. A change from ferromagnetic to antiferromagnetic coupling interchanges the excited dimer states $\Gamma_2^{(1)}$ and $\Gamma_2^{(2)}$, see figure 3. Since the number of Ho^{3+} dimers with their axis along a and b are equal, there is a complete cancellation of the Q dependence of the structure factor, see figure 4. A comparison of the observed dimer splitting with figure 3 therefore yields $\mathcal{J}_a = -\mathcal{J}_b = 1.3 \pm 0.2\ \mu$eV. From these values we calculate the molecular-field parameter $\mathcal{J}(0) = 2(\mathcal{J}_a - \mathcal{J}_b)$ to be $5.2 \pm 0.8\ \mu$eV, which is in good agreement with $\mathcal{J}(0) = 5.6\ \mu$eV derived by fitting the zero-field magnetization data [12].

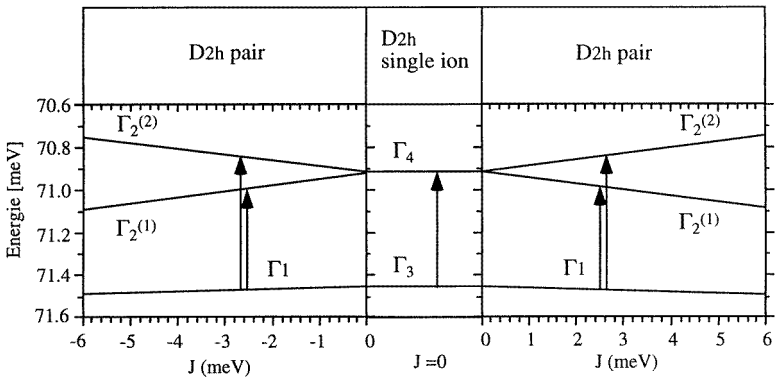

Figure 3. Exchange-induced splitting of the low-lying CEF states of a Ho^{3+} dimer in $Ho_xY_{1-x}Ba_2Cu_3O_7$. The arrows denote the observed transitions.

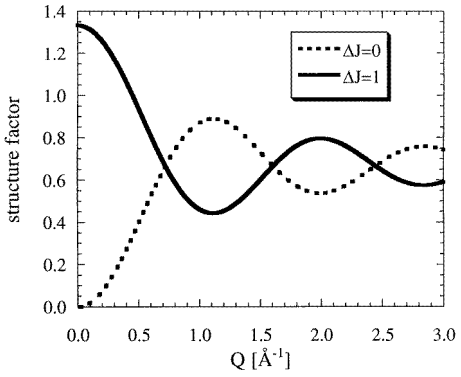

Figure 4. Q dependence of the structure factor $I_{\Delta J}^{\Delta M=\pm 1}(Q)$ of transverse Ho^{3+} dimer excitations in $Ho_xY_{1-x}Ba_2Cu_3O_7$.

5. Collective excitations

In the previous section it was shown that experiments on dimer compounds provide information about the intradimer exchange interaction; however, a more detailed knowledge of the coupling constant is difficult to obtain. The best way to determine the exchange interactions is experiments on single crystals. With the help of inelastic neutron scattering experiments the dispersion of the spin-waves or CEF excitations can be measured. In combination with a model, the exchange couplings can then be deduced. In section 5.1 such a model calculation will be introduced. In sections 5.2 and 5.3 it will be shown how this model can be applied to describe experimental data on $HoBa_2Cu_3O_7$ and $R_{2-x}Ce_xCuO_4$ compounds.

5.1. Random-phase approximation model

In an extended, undiluted system, the spin Hamiltonian is assumed to have the following form:

$$\mathcal{H} = \sum_i \mathcal{H}_{CEF,i} - \sum_{i>j} \hat{\boldsymbol{J}}_i \overline{\overline{\mathcal{J}}}(\boldsymbol{r}_i - \boldsymbol{r}_j)\hat{\boldsymbol{J}}_j \tag{16}$$

where the exchange tensors $\overline{\overline{\mathcal{J}}}(\boldsymbol{r}_i - \boldsymbol{r}_j)$ describe the coupling between the ions at positions $\boldsymbol{r}_i$ and $\boldsymbol{r}_j$, and $\hat{\boldsymbol{J}}_i$ are the total angular momentum operators. In general, the $\overline{\overline{\mathcal{J}}}(\boldsymbol{r}_i - \boldsymbol{r}_j)$ are anisotropic. The many possible causes of two-site exchange anisotropy have been summarized in [15]. In the cases treated below the experiments could be described by a diagonal (HoBaCuO) or even isotropic (NdCuO) exchange tensor. Additionally, anisotropy can be due to crystal-field effects. In this case the angular momentum contribution to $\hat{\boldsymbol{J}}_i$ can lead to single-ion anisotropy.

A convenient way to calculate directly from (16) the wave-vector-dependent susceptibility is the mean-field random-phase approximation (RPA). A description of this method is given in [16]. The approximation consists in neglecting longitudinal fluctuations of $\mathcal{J}_i$, therefore it is clearly best justified when the fluctuations are small, i.e. at low temperatures. The susceptibility for a system with n magnetic ions per magnetic unit cell is given by

$$\chi(\boldsymbol{q}, \omega) = \frac{1}{2}\sum_{rs} \overline{\overline{\chi}}_{rs}(\boldsymbol{q}, \omega) \qquad (r, s = 1, \ldots, n) \tag{17}$$

where the $\overline{\overline{\chi}}_{rs}(\boldsymbol{q}, \omega)$ are the building blocks of the $3n \times 3n$ tensor

$$\overline{\overline{\chi}}(\boldsymbol{q}, \omega) = \begin{pmatrix} \overline{\overline{\chi}}_{11}(\boldsymbol{q}, \omega) & \ldots & \overline{\overline{\chi}}_{1n}(\boldsymbol{q}, \omega) \\ \vdots & \ddots & \vdots \\ \overline{\overline{\chi}}_{n1}(\boldsymbol{q}, \omega) & \ldots & \overline{\overline{\chi}}_{nn}(\boldsymbol{q}, \omega) \end{pmatrix} \tag{18}$$

which has to be determined by the RPA equation

$$\overline{\overline{\chi}}(\boldsymbol{q}, \omega) = (1 - \overline{\overline{\chi}}^0(\omega)\overline{\overline{\mathcal{J}}}(\boldsymbol{q}))^{-1}\overline{\overline{\chi}}^0(\omega). \tag{19}$$

$\overline{\overline{\chi}}^0(\omega)$ is built up of the single-ion susceptibility tensors $\overline{\overline{\chi}}^0_r(\omega)$ $(r = 1, \ldots, n)$:

$$\overline{\overline{\chi}}^0(\omega) = \begin{pmatrix} \overline{\overline{\chi}}^0_1(\omega) & & 0 \\ & \ddots & \\ 0 & & \overline{\overline{\chi}}^0_n(\omega) \end{pmatrix}. \tag{20}$$

For $\omega \neq 0$ the $\overline{\overline{\chi}}^0_r(\omega)$ are given by

$$(\overline{\overline{\chi}}^0_r)^{\alpha\beta}(\omega) = \sum_{\substack{i,j \\ E_i \neq E_j}} \frac{\langle i|\hat{J}^\alpha|j\rangle_r \langle j|\hat{J}^\beta|i\rangle_r}{E_i - E_j - \omega}(p_j - p_i). \tag{21}$$

The exchange coupling tensor is constructed from the Fourier-transformed coupling constants $\overline{\overline{\mathcal{J}}}(\boldsymbol{q})_{r,s}$ $(r, s = 1, \ldots, n)$ of the exchange between ions of sublattices r and s:

$$\overline{\overline{\mathcal{J}}}(\boldsymbol{q}) = \begin{pmatrix} \overline{\overline{\mathcal{J}}}(\boldsymbol{q})_{11} & \ldots & \overline{\overline{\mathcal{J}}}(\boldsymbol{q})_{1n} \\ \vdots & \ddots & \vdots \\ \overline{\overline{\mathcal{J}}}(\boldsymbol{q})_{n1} & \ldots & \overline{\overline{\mathcal{J}}}(\boldsymbol{q})_{nn} \end{pmatrix}. \tag{22}$$

The magnetic excitation energies are the poles of the wave-vector-dependent susceptibility $\chi(\boldsymbol{q},\omega)$. In many cases it is possible to analytically calculate these poles and therefore to determine the dispersion $\omega(\boldsymbol{q})$. For a two-level system with one ion per unit cell, the energies are given by

$$\omega_\alpha(\boldsymbol{q}) = [\Delta^2 - 2M_\alpha^2\Delta(\mathcal{J}_\alpha(\boldsymbol{q})]^{1/2} \tag{23}$$

with $M_\alpha = \langle i|\hat{J}^\alpha|j\rangle$ and $\Delta = E_i - E_j$.

In the case of two ions per unit cell, but identical single-ion susceptibilities (para- or ferromagnet), the energies of the resulting two excitation branches can be expressed by

$$\omega_\alpha(\boldsymbol{q}) = [\Delta^2 - 2M_\alpha^2\Delta(\mathcal{J}_\alpha(\boldsymbol{q}) \pm \nu|\mathcal{J}'_\alpha(\boldsymbol{q})|)]^{1/2}. \tag{24}$$

ν is defined as the sign of $\mathcal{J}'(0)$. $\mathcal{J}_\alpha(\boldsymbol{q})$ and $\mathcal{J}'_\alpha(\boldsymbol{q})$ are the Fourier-transformed intra-sublattice and inter-sublattice exchange functions. The $+$ and $-$ sign corresponds to the acoustic and optical branch, respectively.

In section 5.3 experiments on Nd_2CuO_4 will be discussed, where a noncollinear magnetic order of Nd is observed, which leads to eight magnetic sublattices. Even in this case it is possible to obtain closed expressions for the excitation energies. They are more complex and given elsewhere [17, 18].

The wave-vector-dependent susceptibility can directly be determined by inelastic neutron scattering (see (4)). For a two-level system with one ion per unit cell, the scattering function is given by

$$S^{\alpha\alpha}(\boldsymbol{Q},\omega) = \frac{N\bar{h}}{\pi}\left(1 - \exp\left(-\frac{\bar{h}\omega}{k_B T}\right)\right)^{-1} M_\alpha^2 \frac{\Delta}{\omega_\alpha(\boldsymbol{q})}. \tag{25}$$

In the case of two ions per unit cell, but identical single-ion susceptibilities (para- or ferromagnet) it can be expressed by

$$S^{\alpha\alpha}(\boldsymbol{Q},\omega) = \frac{N\bar{h}}{2\pi}\left(1 - \exp\left(-\frac{\bar{h}\omega}{k_B T}\right)\right)^{-1} M_\alpha^2 (1 \pm \cos\varphi) \frac{\Delta}{\omega_\alpha(\boldsymbol{q})}. \tag{26}$$

The $+$ and $-$ sign corresponds to the acoustic and optical branch, respectively, and the phase φ is defined through $\mathcal{J}'(\boldsymbol{Q}) = \mathcal{J}'(\boldsymbol{q})\exp(-\mathrm{i}\tau\cdot\boldsymbol{r}) = \nu|\mathcal{J}'(\boldsymbol{q})|\exp(-\mathrm{i}\varphi)$, with $\tau = \boldsymbol{Q} - \boldsymbol{q}$ the reciprocal lattice vector and $\boldsymbol{r}$ a vector connecting the two sublattices.

In the case of the noncollinear magnetic structure of the Nd ions in Nd_2CuO_4 closed expressions for $S(\boldsymbol{Q},\omega)$ are given in [17].

5.2. Experiments on $HoBa_2Cu_3O_7$ grain-aligned samples

The most convenient way for an investigation of the exchange interactions of Ho in $HoBa_2Cu_3O_7$ would be a measurement of the dispersion of the Γ_3–Γ_4 CEF excitations in a single crystal. Unfortunately no sufficiently large and perfect crystals are available so far. A different approach is a measurement on grain-aligned samples [19], which provides more detailed information on the exchange interactions between the Ho ions than the powder experiment presented in section 4.

The method of producing such samples consists in applying a magnetic field on a polycrystalline sample mixed into heptane and sarcosyl-O. The grains then align along the easy axis of magnetization, which in case of $HoBa_2Cu_3O_7$ is the z axis at room temperature. The organic material is evaporated after the alignment. The rocking curve for $(00l)$ has then a half-width at half-maximum of typically 10°. The a and b axes remain of course randomly oriented. Therefore it is impossible to distinguish between the in-plane components of a

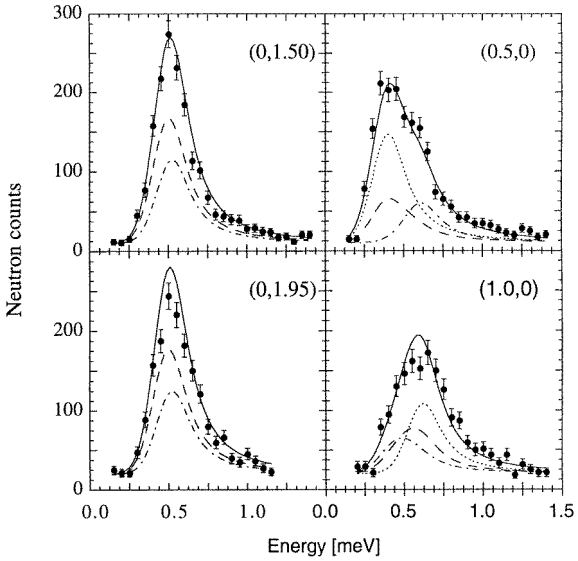

Figure 5. Normalized and form-factor-corrected energy spectra of neutrons scattered from grain-aligned $HoBa_2Cu_3O_7$ at 1.5 K for $\boldsymbol{Q}$ parallel and perpendicular to the c axis. The full lines correspond to the calculated excitation spectra as explained in the text. The broken, dash–dotted and dotted lines represent x, y and z polarizations, respectively.

Table 1. Refined parameters for both anisotropic and isotropic magnetic coupling in $HoBa_2Cu_3O_7$.

Anisotropic model	Isotropic model
$\mathcal{J}^a_\perp = 3.2 \pm 0.7\ \mu$eV	
	$\mathcal{J}^a = 2.2 \pm 1.1\ \mu$eV
$\mathcal{J}^a_\parallel = 0 \pm 0.2\ \mu$eV	
$\mathcal{J}^b_\perp = -2.4 \pm 0.8\ \mu$eV	
	$\mathcal{J}^b = -2.4 \pm 1.2\ \mu$eV
$\mathcal{J}^b_\parallel = -6.9 \pm 1.6\ \mu$eV	
$\Delta = 0.52 \pm 0.02$ meV	$\Delta = 0.52 \pm 0.02$ meV
$M_x^2 = 11.4 \pm 2.4$	$M_x^2 = 14 \pm 0.5$
$M_y^2 = M_z^2 = 7.8 \pm 1.2$	$M_y^2 = M_z^2 = 6.5 \pm 2.5$
$\chi^2 = 2.4$	$\chi^2 = 3.3$

reciprocal lattice vector $\boldsymbol{Q} = 2\pi(h/a, k/b, l/c)$, and one introduces an actual scattering vector $\boldsymbol{Q} = 2\pi(h'/a, l/c)$, with $h' = \sqrt{h^2 + k^2}$, assuming $a = b$.

Figure 5 shows four out of twenty-one spectra of the experiments performed on the cold triple-axis spectrometer V2 installed at the Hahn-Meitner-Institute Berlin. Because one is dealing with a two-level system, the energies and intensities of the excitations are given by (23) and (25), respectively. The Fourier-transformed coupling constant is given by

$$\mathcal{J}_\alpha(\boldsymbol{q}) = 2\mathcal{J}^a_\alpha \cos(2\pi h) + 2\mathcal{J}^b_\alpha \cos(2\pi k) + 2\mathcal{J}^c_\alpha \cos(2\pi l) \tag{27}$$

where $\mathcal{J}^a_\alpha$, $\mathcal{J}^b_\alpha$ and $\mathcal{J}^c_\alpha$ denote the exchange couplings between nearest-neighbour ions

along the a, b and c direction, respectively. Due to the mixing of different $\boldsymbol{Q}$ vectors in the plane, the dispersion cannot directly be deduced from these experiments. One has to fit simultaneously all the spectra, while doing a proper superposition of the excitations in the (x, y) plane. The lines in figure 5 show the results of this fitting procedure. The origin of the asymmetric line-shape is still an open question. It is also observed in highly diluted compounds, which shows that it is a single-ion effect (see figure 2(c)).

From the absence of a dispersion along the c direction it follows directly that $\mathcal{J}_\alpha^c \approx 0$. This proves that the assumption made in section 3 of negligible exchange coupling along the c direction is justified. In table 1 the results of the investigation are shown, for both isotropic and anisotropic exchange interactions. The Heisenberg model is clearly inferior to the model with anisotropic magnetic coupling parameters. There is a good agreement of these coupling constants to the ones determined by dimer excitations.

5.3. Experiments on $Nd_{2-x}Ce_xCuO_4$ single crystals

In contrast to the $RBa_2Cu_3O_7$ compounds, there are large enough $R_{2-x}Ce_xCuO_4$ single crystals available for inelastic neutron scattering investigations. The first such experiment was a determination of the dispersion of the Pr Γ_4–Γ_5 CEF excitation in Pr_2CuO_4 [20]. In this compound no spin-waves can be observed because the CEF ground state is a singlet. Here the results of inelastic neutron scattering investigations of the spin-waves and the dispersion of CEF excitations in $Nd_{2-x}Ce_xCuO_4$ are discussed.

In Nd_2CuO_4, the tenfold degenerate $J = 9/2$ ground-state multiplet of Nd is split by the CEF interaction into a magnetic ground-state doublet ($\Gamma_6^{(1)}$) and four Kramers doublets at 14 meV ($\Gamma_7^{(1)}$), 21 meV ($\Gamma_6^{(2)}$), 27 meV ($\Gamma_7^{(2)}$) and 93 meV ($\Gamma_6^{(3)}$) [21–26]. The exchange interaction between the Nd leads to a dispersion of these levels. Due to the two-ion basis of the Nd in this substance, one observes two excitation branches (see (24)). Figure 6 shows the results of measurements performed on the triple-axis spectrometer IN8 at the Institute Laue–Langevin, Grenoble [27]. As expected from (24), the dispersion for the $\Gamma_6^{(1)}$–$\Gamma_6^{(2)}$ CEF transition is larger than for the $\Gamma_6^{(1)}$–$\Gamma_7^{(2)}$ CEF transition due to the bigger matrix element. Figure 7 shows the measured dispersion of the $\Gamma_6^{(1)}$–$\Gamma_6^{(2)}$ CEF excitation. The lines correspond to the model calculation. The energies (24) as well as the intensities (26) are perfectly described with one set of exchange constants, which are indicated in figure 8, and have the following size:

$$\mathcal{J}_1 = -7\ \mu\text{eV} \qquad \mathcal{J}_2 = -19\ \mu\text{eV} \qquad \mathcal{J}_3 = -2.5\ \mu\text{eV}.$$

Below the Nd ordering temperature of approximately 1.5 K, spin-waves are observed [18, 28, 29]. These excitations can be regarded as transitions within the ground-state doublet, which is split by the exchange field. Figure 9 shows a measurement of spin-wave excitations performed on the triple-axis spectrometer V2 installed at the Hahn-Meitner-Institute, Berlin [28]. Because of the low ordering temperature, a dilution refrigerator was used. Due to the noncollinear AF structure [30] with eight magnetic Nd sublattices (four per chemical sublattice) the spin-wave dispersion consists of eight modes, four acoustical (A) and four optical (O) branches. Figure 10 shows the determined dispersion [28]. To index the positions in reciprocal space the magnetic unit cell which is obtained by a $\sqrt{2} \times \sqrt{2}$ expansion and 45 degree rotation of the chemical unit cell basal plane is used. The lines correspond to a model calculation [17, 18]. The model gives a good description of the energies as well as of the intensities. Figure 11 shows the measured and calculated intensity of the optic branch along [001], normalized to the total magnetic scattering. A broadening of lines observed at some reciprocal lattice positions indicates that the degeneracy of the excitations may be

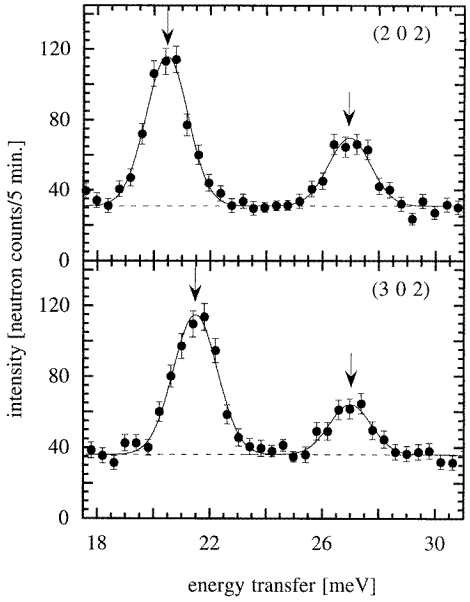

Figure 6. Energy spectra of neutrons scattered from Nd_2CuO_4 at 4 K for two different $\boldsymbol{Q}$ positions.

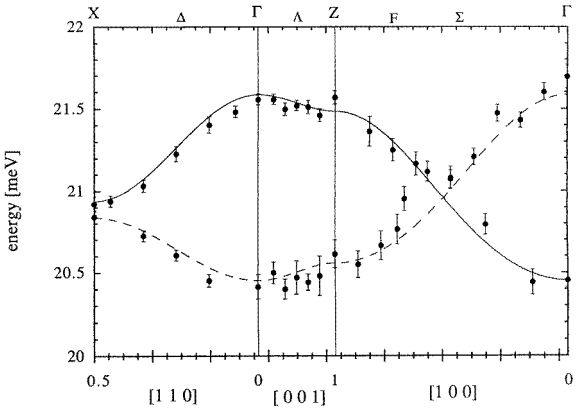

Figure 7. Measured dispersion of the $\Gamma_6^{(1)}$–$\Gamma_6^{(2)}$ Nd CEF excitation in Nd_2CuO_4 at 4 K. The lines correspond to the RPA model calculation (——, acoustic branch; — — —, optic branch).

further lifted than predicted by the model calculation. A possible reason for this could be a small tilting ($\approx 1^\circ$) of the Nd with respect to Cu moments [17].

The large gap of the spin-waves originates from the Nd–Cu exchange interaction which creates a staggered magnetic field $h_{cu} \approx 0.5$ meV at the Nd site. The Nd–Nd exchange constants which lead to the dispersion have the following size:

$$\mathcal{J}_1 = -33\ \mu\text{eV} \qquad \mathcal{J}_2 = 18\ \mu\text{eV} \qquad \mathcal{J}_3 = -8\ \mu\text{eV} \qquad \mathcal{J}_4 = -4\ \mu\text{eV}.$$

Note that these exchange constants, especially $\mathcal{J}_2$, differ from the ones obtained previously [31] with another model [32]. Here a description is used where the difference

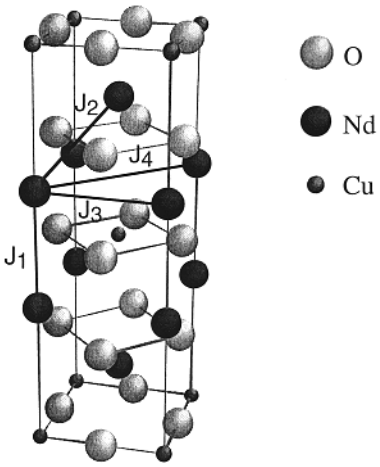

Figure 8. Crystal structure of Nd_2CuO_4 with the various Nd–Nd exchange constants indicated.

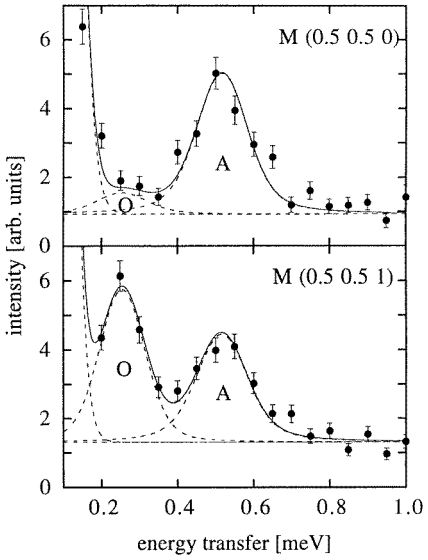

Figure 9. Energy spectra of neutrons scattered from Nd_2CuO_4 at $T = 50$ mK at two different M points. A stands for the acoustic, O for the optic excitation. The lines are the result of a least-squares fitting procedure as explained in the text.

of the single-ion susceptibilities in the eight magnetic sublattices is explicitly taken into account. Recently a model has been presented where the interactions of the Cu spins have been included [33]. The two dispersions deviate however only close to the gamma point. Moreover, four-site exchange interactions may lead to Cu spin gaps [34] which have indeed been observed at 12 meV and 14 meV at 5 K [20, 35, 36]. This justifies the assumption that the only consequence of the Cu–Nd exchange interaction is the creation of a staggered magnetic field at the Nd site. The case is different for the $\Gamma_6^{(1)}$–$\Gamma_6^{(2)}$ CEF excitation. At approximately 21 meV, Cu spin-waves are unquestionably present. We performed a numerical calculation of the wave-vector-dependent susceptibility including

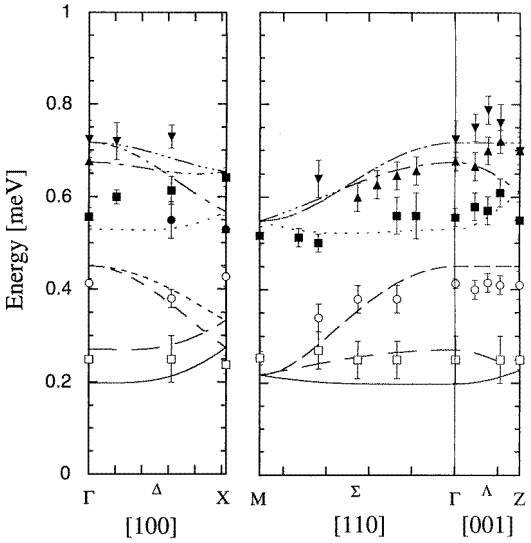

Figure 10. Measured dispersion of the Nd spin-waves in Nd_2CuO_4 at $T = 50$ mK. The lines correspond to the model calculation with the exchange constants given in the text.

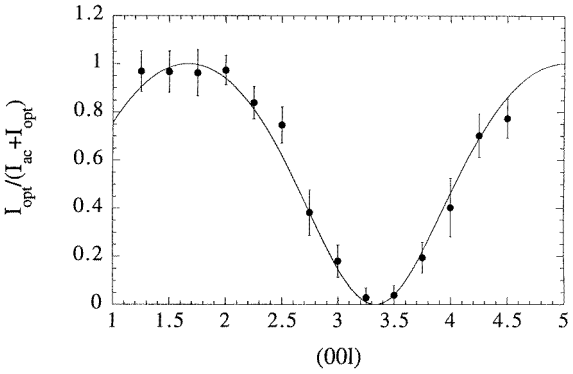

Figure 11. Measured intensity of the optic spin-wave branch along [001], normalized to the total magnetic scattering. The line corresponds to the RPA model calculation.

Cu–Cu, Cu–Nd and Nd–Nd exchange interaction. The result shows that the dispersion of the CEF excitation is indeed affected at the X point, where the Cu spin-waves cross the CEF level. The anomaly at this point is however only small, and could not be resolved by neutron scattering experiments. Apart from that, the results of these calculations correspond to (24).

Remarkably the exchange constants of the spin-wave dispersion considerably deviate from the ones of the CEF excitation. This shows that the exchange interaction is dependent on the initial and final state of a transition. This has also been observed in the case of a dimer compound [37].

Finally the results of experiments on Ce-doped samples are presented [38]. In figure 12 the spectra of doped samples at a temperature of 50 mK at $\boldsymbol{Q} = (0\ 0\ 1.5)$ are compared with the spectrum of the undoped sample. The lines correspond to damped harmonic oscillators

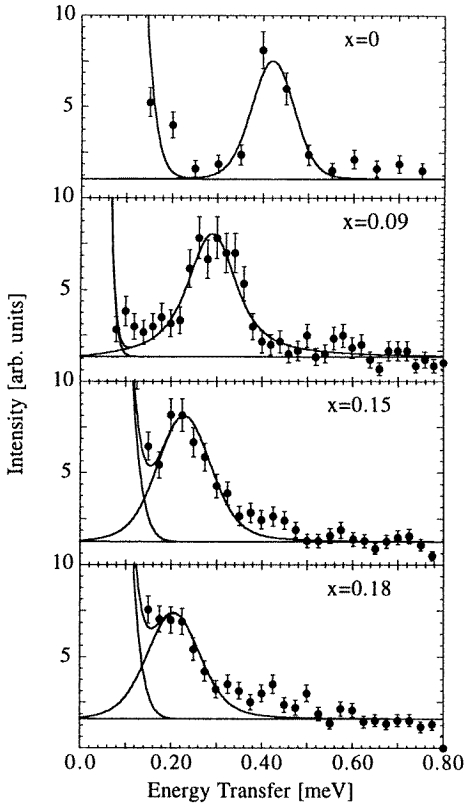

Figure 12. Spectra of neutrons scattered from $Nd_{2-x}Ce_xCuO_4$ ($x = 0, 0.09, 0.15, 0.18$) at $T = 50$ mK and $\boldsymbol{Q} = (0\ 0\ 1.5)$.

convoluted with the resolution function. It is obvious that there is a significant softening of the spin-wave excitations upon Ce doping. Figure 13 shows the excitation energies as a function of doping for a selection of four different momentum transfers. The same amount of softening is observed for all the measured excitations at all $\boldsymbol{Q}$ positions where experiments have been performed. This implies that the splitting of the spin-wave branches remains constant for all doping levels. Because this splitting is defined by the Nd–Nd exchange interaction, this signifies that the Nd–Nd exchange constants are almost unaffected by the doping process. The softening must therefore originate from the reduction of the Nd–Cu exchange field at the Nd site. This reduction is easily explained by the decrease of the Cu magnetic moment due to the doping of electrons into the copper oxide planes. The very small line-widths of the excitations indicate that the samples are very homogeneously doped. An inhomogenous doping would lead to a distribution of different sizes of Cu moments, and consequently to varying Cu–Nd exchange fields at the Nd site. In an $x = 0.13$ compound a large line-width was indeed observed [38], indicating a bad sample quality.

The effect of the observed softening of spin-wave branches for the specific heat can easily be calculated. The softening shifts the spin-wave branches and accordingly the peaks in the density of states to lower values. At a critical Nd–Cu exchange field, corresponding to $h_{Cu} = 0.38$ meV in the calculation, one spin-wave branch shows a complete softening. In figure 14 the density of states for $h_{Cu} = 0.52$ meV and $h_{Cu} = 0.38$ meV is shown. In

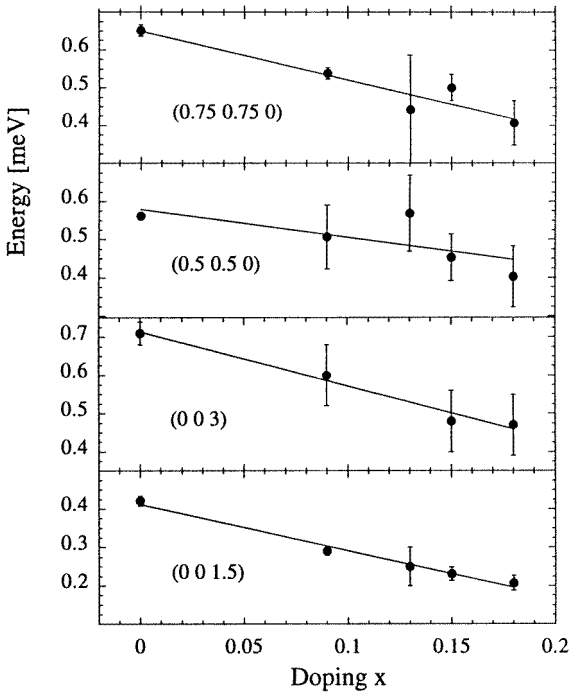

Figure 13. Energies of the spin-wave excitations of Nd in $Nd_{2-x}Ce_xCuO_4$ as a function of Ce doping at different positions in reciprocal space.

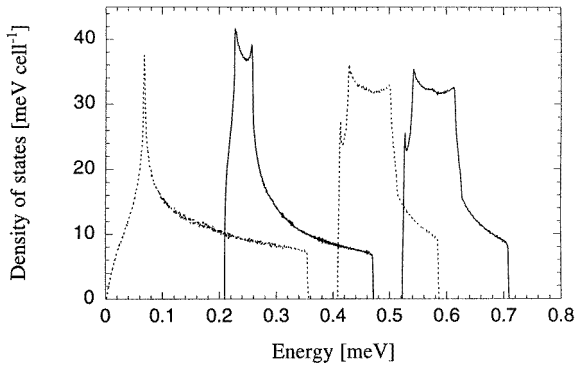

Figure 14. Density of states of the spin-wave excitations. ——, $h_{Cu} = 0.52$ meV; - - - -, $h_{Cu} = 0.38$ meV.

figure 15 the calculated $\gamma = C/T$ values for three different h_{Cu} are shown and compared with the experimental results of Brugger *et al* [4]. Note that the spin-wave model is only valid for $T \ll h_{MF}/k_B \approx 5$ K, where h_{MF} is the combined Nd–Cu and Nd–Nd exchange field. For values of h_{Cu} lower than 0.38 meV the observed continuation of the spin-wave softening upon further doping will lead to an even higher density of states at low energies, and consequently to the observed higher γ values. This clearly shows that the Nd–Nd correlations significantly affect the specific heat and explain the high γ values.

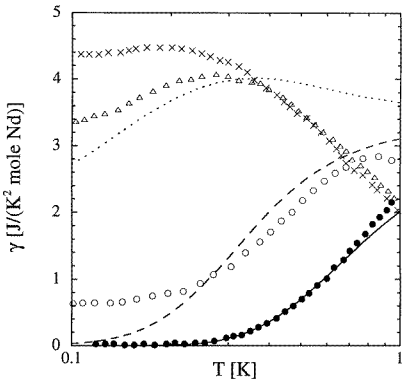

Figure 15. Specific heat coefficient $\gamma = C/T$. Symbols correspond to experimental data of Brugger *et al* [4]: ●, $x = 0$; ○, $x = 0.1$; Δ, $x = 0.15$; ×, $x = 0.2$. The lines show calculations described in the text: ——, $h_{Cu} = 0.50$ meV, — — —, $h_{Cu} = 0.42$ meV; - - - -, $h_{Cu} = 0.39$ meV.

6. Conclusions

We have shown that INS is a unique tool to determine the electronic ground state of the R^{3+} ions as well as the magnetic coupling between the R^{3+} ions in superconducting materials containing rare-earth ions. Experiments on polycrystalline material are sufficient to achieve a precise knowledge of the CEF interaction as well as the intra-dimer coupling at low R concentration as demonstrated for $Ho_xY_{1-x}Ba_2Cu_3O_7$. More detailed information on the magnetic coupling between the R^{3+} ions requires the use of ordered crystalline materials which may be either partially ordered (grain-aligned samples) or more preferably completely ordered (single crystals). The magnetic coupling between the R^{3+} ions gives rise to a dispersion behaviour of the spin excitations which can be measured over the whole Brillouin zone. The RPA theory has proven to be a very efficient tool to describe such measurements. Analysing the experimental data the RPA model yields direct information on the exchange couplings between the rare-earth magnetic moments. This allows the calculation of the density of states of magnetic excitations and consequently of thermodynamic properties like the specific heat. This was demonstrated in detail for the compound $Nd_{2-x}Ce_xCuO_4$ in which a softening of the spin waves upon doping with Ce was observed. Spin-wave softening leads to enhanced $\gamma = C/T$ values which very well explain the heavy-fermion-like behaviour reported in these substances.

Acknowledgments

Financial support by the Swiss National Science Foundation is gratefully acknowledged. For their participation in the experimental and theoretical work as well as for numerous stimulating discussions we are grateful to our colleagues F Fauth, U Staub, P Vorderwisch, B Roessli, J Mesot, P Thalmeier and Tapan Chatterji.

References

[1] Wu M K, Ashburn J R, Torng C J, Hor P H, Meng R L, Gao L, Huang Z J, Wang Y Q and Chu C W 1987 *Phys. Rev. Lett.* **58** 908

[2] Cava R J, Batlogg B, van Dover R B, Murphy D W, Sunshine S A, Siegrist T, Remeika J P, Rietman E A, Zahurak S and Espinosa G P 1987 *Phys. Rev. Lett.* **58** 1676
[3] Tokura Y, Takagi H and Uchida S 1989 *Nature* **337** 345
[4] Brugger T, Schreiner T, Roth G, Adelmann P and Czjzek G 1993 *Phys. Rev. Lett.* **71** 2481
[5] Lovesey S W 1987 *Theory of Neutron Scattering from Condensed Matter (International Series of Monographs on Physics 72)* vol 2 (Oxford: Clarendon)
[6] van Hove L 1954 *Phys. Rev.* **93** 268
[7] Johnston D F 1966 *Proc. Phys. Soc.* **88** 37
[8] Judd B R 1963 *Operator Techniques in Atomic Spectroscopy (Advanced Physics Monograph Series)* (New York: McGraw-Hill)
[9] Mesot J and Furrer A 1997 *J. Supercond.* **10** 623
[10] Staub U, Mesot J, Guillaume M, Allenspach P, Furrer A, Mutka H, Bowden Z and Taylor A D 1994 *Phys. Rev.* B **50** 4068
[11] Furrer A, Brüesch P and Unternährer P 1988 *Phys. Rev.* B **38** 4616, and references therein
[12] Roessli B, Fischer P, Staub U, Zolliker M and Furrer A 1993 *Europhys. Lett.* **23** 511
[13] Guillaume M, Staub U, Fauth F, Mesot J, Furrer A and Carlile C J 1994 *Physica* C **223** 333
[14] Furrer A, Güdel H U and Darriet J 1985 *J. Less-Common Met.* **111** 223
[15] Jensen J, Houmann J G and Møller H B 1975 *Phys. Rev.* B **12** 303
[16] Jensen J and Mackintosh A R 1991 *Rare Earth Magnetism, Structures and Excitations* (Oxford: Clarendon)
[17] Thalmeier P 1997 *Preprint*
[18] Metz A unpublished
[19] Fauth F, Staub U, Guillaume M, Mesot J, Furrer A, Dosanjh P, Zhou H and Vorderwisch P 1995 *J. Phys.: Condens. Matter* **7** 4215
[20] Sumarlin I W, Lynn J W, Chattopadhyay T, Barilo S N and Zhigunov D I 1995 *Phys. Rev.* B **51** 5824
[21] Staub U, Allenspach P, Furrer A, Ott H R, Cheong S-W and Fisk Z 1990 *Solid State Commun.* **75** 431
[22] Hoffmann P, Loewenhaupt M, Horn S, van Aken P and Jostarndt H-D 1992 *Physica* B **163** 10 075
[23] Boothroyd A T, Doyle S M, Paul D M and Osborn R 1992 *Phys. Rev.* B **45** 10 075
[24] Loong C K and Soderholm L 1993 *Phys. Rev.* B **48** 14 001
[25] Loewenhaupt M, Fabi P, Horn S, van Aken P and Severing A 1995 *J. Magn. Magn. Mater.* **140–144** 1293
[26] Jandl S, Dufour P, Strach T, Ruf T, Cardona M, Nekvasil V, Chen C and Wanklyn B M 1995 *Phys. Rev.* B **52** 15 558
[27] Henggeler W, Chattopadhyay T, Roessli B, Zhigunov D I, Barilo S N and Furrer A 1996 *Z. Phys.* B **99** 465
[28] Henggeler W, Chattopadhyay T, Roessli B, Zhigunov D I, Barilo S N and Furrer A 1996 *Europhys. Lett.* **34**
[29] Casalta H, Bourges P, Petitgrand D and Ivanov A 1996 *Solid State Commun.* **100** 683
[30] Skanthakumar S, Lynn J W, Peng J L and Li Z Y 1993 *Phys. Rev.* B **47** 6173
[31] Henggeler W, Chattopadhyay T, Roessli B, Vorderwisch P, Thalmeier P, Zhigunov D I, Barilo S N and Furrer A 1997 *Phys. Rev.* B **55** 1269
[32] Thalmeier P 1996 *Physica* C **266** 89
[33] Sachidanandam R, Yildirim T, Harris A B, Aharony A and Entin-Wohlman O 1997 *Phys. Rev.* B **1997** 260
[34] Sobolev V L, Huang H L, Pashkevich Y G, Larionov M M, Vitebsky I M and Blinkin V A 1994 *Phys. Rev.* B **49** 1170
[35] Bourges P, Ivanov A S, Petitgrand D, Rossat-Mignod J and Boudarene L 1993 *Physica* B **186** 925
[36] Ivanov A S, Bourges P, Petitgrand D and Rossat-Mignod J 1995 *Physica* B **213** 60
[37] Furrer A, Güdel H U, Krausz E R and Blank H 1990 *Phys. Rev. Lett.* **64** 68
[38] Henggeler W, Roessli B, Furrer A, Vorderwisch P and Chatterji T 1998 *Phys. Rev. Lett.* **80** 1300